Axonal Transport Velocity Estimation from Kymographs Based on Curvilinear Feature Extraction and Spline Fitting

Alka Nair[1], Sriprabha Ramanarayanan[2], Shikha Ahlawat[3]
Sandhya Koushika[4], Niranjan Joshi[2], Mohanasankar Sivaprakasam[1,2]

***Abstract*— Axonal transport velocities are obtained from spatio-temporal maps called kymographs developed from time-lapse confocal microscopy movies of neurons. The kymographs of axonal transport of *C.elegans* worms are much noisier due to in vivo nature of imaging. Existing methodologies for velocity measurement include laborious manual delineation of axonal movement ridges on the kymographs and thereby determining particle velocities from the slopes of ridges marked. Manual kymograph analysis is not only time consuming but also prone to human errors in marking the ridges. An automated algorithm to extract all the ridges and determine the velocities without significant manual efforts is highly preferred. Not many methods are currently available for such biological studies. We present an almost automated method based on information fusion using LDA classifier, morphological image processing and spline fitting for determining axonal transport velocities. Experimental analysis of 50 kymographs shows considerable reduction of 89% in time taken with manual intervention of 10.83%. Comparitive study with the results of two of the previous literatures shows that our algorithm performs better.**

I. INTRODUCTION

Axonal transport is an essential cellular process which has been shown to play a key role in various neurodegenerative diseases. Biologists working in the area of axonal transport are still widely investigating the role of transport characteristics like velocity, flux, pause time and pause frequency for such diseases. Time lapse confocal microscopy is used for imaging this transport phenomenon. The captured movie is converted to a spatio-temporal map called kymograph which encodes the position of particle at a given point of time. Moving particles are represented as slant lines whose slope gives the velocity of the particle. Stationary particles are seen as vertical lines. We propose a method to quantify axonal transport velocity from kymographs which when compared to manual analysis, takes lesser time and effort.

II. A BRIEF REVIEW OF PREVIOUS RESEARCH

The manual analysis of kymograph is not only laborious and time consuming task but also prone to human errors and hence automating the process is of much significance to the biologists. We have used kymographs with vesicles of *C.elegans* (a worm) as the transport particle. Various methods have been proposed in recent years for automated analysis of axonal transport using kymograph generation and tracking algorithms. However, these algorithms are not robust enough for *C.elegans* movies with noisy kymographs. *C.elegans* are used as model organisms because of their transparent structure that facilitates live/in vivo imaging. The neuron diameter of *C.elegans* is of the order of 300 nm. This creates a heavy traffic in the axon wherein the particle count is high resulting in a kymograph with a large number of curvilinear structures which are difficult to discern. The size of the *C.elegans* vesicles is also small, of the order of 30-40 nm, which in turn provides lesser surface area for fluorescent proteins like Green Fluorescent Protein (GFP) to tag. These particles are imaged at a poor x-y resolution of 280nm. Movies are captured at 5 frames/second which results in low signal to noise ratio (SNR). The intensity-based algorithm presented in [1] requires very high spatial resolution of kymographs. The method presented in [2] works on particles bigger than *C.elegans* vesicles and the kymographs had high SNR. The automated velocity measurement approaches in [3] and [4] based on image cross and auto correlation of the kymograph columns and Hough transforms are not suitable for high noise levels. Algorithms in [5] and [6] using Stegers edge detection are unable to trace faint ridges. Comparison of kymographs of *C.elegans* movie with the kymograph from [5] shows that particle movement is more heterogenous in the *C.elegans* kymograph. We tried our algorithm on kymographs from [5] and [6] . The edge result from the paper and our algorithm shows that our algorithm detects more number of true edges as shown in Fig. 1 and Fig. 2. In [9], the kymograph generation algorithm works well only when the axon of the worm lies horizontally. We have used ImageJ plugins for kymograph generation.

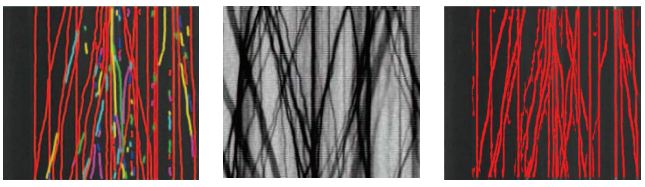

(a) (b) (c)

Fig. 1: (b) shows kymograph from [5]. (a) shows result of [5]. (c) shows result of proposed method on (b). The red lines are the detected lines by algorithm. The rest of the colours show missed out lines.

[1] Department of Electrical Engineering, IIT Madras, India
[2] Healthcare Technology Innovation Centre, IITM Research Park, Chennai, India
[3] National Center for Biological Sciences, Bangalore, India
[4] Dept.of Biologial Sciences, TIFR, Mumbai, India

978-1-4244-7929-0/14/$26.00 ©2014 IEEE

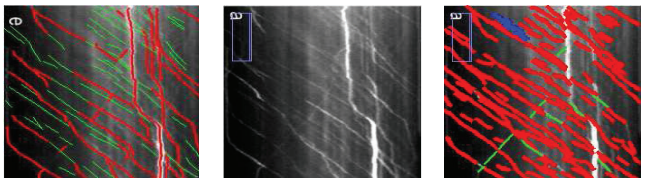

(a) (b) (c)

Fig. 2: (b) is a kymograph from the article [6]. (a) and (b) are the results from [6] and our algorithm respectively. The red lines indicate the ones detected by algorithm. Green lines are the undetected lines. The blue lines are the falsely detected lines. From the figure, it is clear that the number of true positive edges detected by our algorithm are more than that shown in [6].

III. Challenges in Automating the Analysis of Kymographs

The challenges of existing methodology routinely used by biologists are: 1) manual delineation of edges by zooming the image 2) poor slant ridge intensities and high background noise and 3) high intensities of vertical lines of stationary particles amongst the slant lines to be extracted. Hence the slant lines of interest i.e., the anterograde and retrograde (particles moving towards cell body and synapse respectively) movements need to be enhanced and background noise suppressed.

IV. Material and Methods

We have used the transgenic jsls821(wild type or the normal phenotype) of *C.elegans* expressing GFP::RAB3 in synaptic vesicles of the touch neurons. The kymograph has distance along the x-axis and time along the y-axis. The algorithm has the 3 main modules - 1. Information fusion based on Linear Discriminant Analysis (LDA) 2. Post processing and 3. Velocity estimation

Classification: Classification involves training and testing. The training phase requires feature specification of slant lines as foreground and other regions as background. The feature images for training are derived by using various feature extraction methods applied to 8 kymographs. 50 kymographs are used for testing. The 6 best features chosen empirically for training are Gabor filtered image, Frangi vesselness measure, Frangi vesselness of Gabor image, a hybrid vesselness measure using Gabor and Frangi, Top-hat transform of Gabor image and Anisotropic diffusion of Gabor image. Gabor filters are sinusoidally modulated Gaussian functions . The real Gabor filter kernel oriented at the angle $\theta = \frac{\pi}{2}$ is formulated as

$$g(x,y) = \frac{1}{2\pi\sigma_x\sigma_y} exp(-\frac{1}{2}(\frac{x^2}{\sigma_x^2} + \frac{y^2}{\sigma_y^2})) \cos(2\pi f_0 x) \quad (1)$$

where σ_x and σ_y are the standard deviations along the x and y directions respectively and f_0 is the frequency of the modulating sinusoid. $\sigma_x = \frac{\tau}{2\sqrt{2\ln 2}}$, where τ is the thickness of the line segment and $\sigma_y = lx$, where l determines the elongation of the Gabor filter in the orientation direction w.r.t. its thickness [7]. We rotate this kernel to enhance curvilinear structures at different orientations. The maximum response across all the orientations is called the Gabor image. The vesselness measure proposed by Frangi in [8] is given as

$$v_0(s) = \begin{cases} 0 & \lambda_2 > 0 \\ exp(-\frac{R_B^2}{2\beta^2})(1 - exp(-\frac{S^2}{2c^2})) & otherwise \end{cases} \quad (2)$$

where R_B differentiates lines from blobs, S is the Frobenius norm, and parameters β and c are the weighing factors. Two features are derived from Frangi vesselness. One is the vesselness map on the original kymograph and the other is the vesselness map on the Gabor image. The Frangi vesselness map of Gabor has the advantage that it combines the enhancement property of Gabor filter and Frangi vesselness along with the background suppression of the Frangi vesselness. This has also helped in enhancing the very faint curvilinear structures present in the image. The hybrid measure of Gabor and Frangi makes use of the vesselness function of Frangi but the two eigen values are now replaced with the magnitude of Gabor along the vessel direction and the average magnitude along all other directions except for vessel direction. This method proves to provide a more enhanced feature than Frangi vesselness. The Top-hat transformation of the Gabor filtered image is done in all the directions using a line structuring element and the maximum response is found out. Both positive and negative classes are hand drawn on all 8 images. Pixels depicting the slant lines are marked as positive. Those pixels that belong to the bright vertical lines (stationary particles) and homogeneous background region are labelled as negative. After training phase, a test kymograph image is given to the LDA classifier. A probability map is generated by the classifier for the test image which shows the probability of each pixel belonging to a curvilinear structure.

Post-processing: The post-processing algorithm is used to extract entire curvilinear ridge features from the probability map, remove noisy and false positive edges and fit smoothing splines on the extracted ridges. Curvilinear ridges are extracted by repeated morphological opening with oriented line structuring elements (Fig. 3). For anterograde ridges, the line structuring elements are oriented along directions from 100° - 170° with respect to the positive X-axis. For retrogrades ridges, the structuring elements are oriented along 10-80°. Each opening operation enhances the slant curvilinear ridges with respect to the background. The ridge image obtained by summing up all the opened images yields high ridge responses and low noise and background intensities. The ridge image so obtained is denoised by Frangi vesselness filter and binary thresholded to extract all the prominent edges. In order to retain only the curvilinear structures, we perform morphological reconstruction by geodesic dilation on each connected component of the binary image. Reconstruction ensures that false and noisy ridges are eliminated. Erosion of the connected components by a slanted (45 and 135 degrees) line structuring element yields the marker image for reconstruction. The reconstructed binary image has all

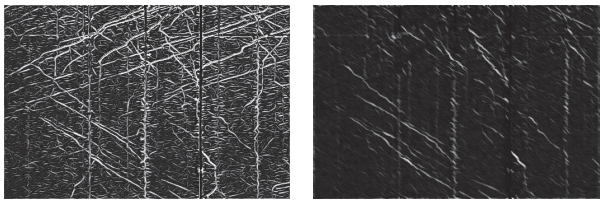

(a) (b)

Fig. 3: (a) shows a probability map. (b) shows the result of repeated morphological openings for anterograde components.

the slant ridges that contribute to velocity computations. However in some ridges, the presence of horizontal or vertical lines due to discretisation artifact causes the slope along that segment to be 0 or infinity respectively. Some of the ridges are jagged leading to incorrect slope value. This problem is solved by fitting a smoothing spline with smoothing parameter 0.05 to the ridge, as shown in (Fig. 4), so that variations are smooth and continuous, thereby enabling the possibility of obtaining instantaneous velocities and acceleration values.

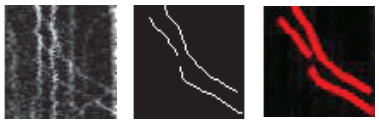

(a) (b) (c)

Fig. 4: (a) is the original kymograph. (b) is the image after postprocessing. (c) shows the fitted spline on the anterograde ridges.

Velocity computation: For each component, the x-coordinates of the spline are the column pixel positions on the image. The corresponding y-coordinate positions (row pixel positions) are evaluated from the spline curve. The following steps are followed in velocity computations. a. Compute the coordinate values of x_i and y_i at equally spaced points on the curve by spline interpolation. b. Slope of the nth point on the curve is, $Slope(n) = (y_{n+1} - y_n)/(x_{n+1} - x_n)$. c. For each slope value the corresponding velocity is computed as, $Velocity = (1/slope)$ d. Overall velocity = mean of all velocity values on the all the curves on the image.

Removal of intersecting ridge components and spurious branches: A continuous set of points without branches is required as otherwise spline fitting would render a curve that goes in between the branches. Spurious ridges and branches are removed by identifying the two farthest end points and the intermediate branch points as shown in Fig. 5. These points are joined by using Dijkstra's algorithm. This method is preferred over morphological pruning which can be used only if the branches are small. Also, repeated pruning operation reduces the length of the main trunk and hence is not helpful.

V. Results and Discussion

Our algorithm is evaluated in terms of the time taken for manual efforts versus semi-automated method, velocity

(a) (b) (c) (d) (e) (f)

Fig. 5: (a) Connected component with a branch. (b) spline fitting on this component gives an incorrect curve that passes in between the branching ridges 2D plot of the spline curve fit of a connected component. (c) Removing the junction point disconnects the component into three short components making them insignificant for velocity computations. (d) Farthest end points and intermediate junction points. (e) Main trunk obtained from Dijkstra's algorithm. (f) Spline curve fitting on (d).

comparisons and error analysis for 50 kymographs. The final result depicting the lines detected by the algorithm is shown in Fig. 6.

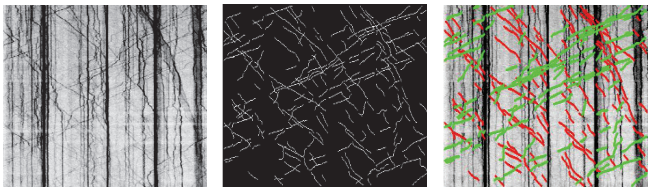

(a) (b) (c)

Fig. 6: (a) is the inverted contrast adjusted original kymograph. (b) is the result of the proposed algorithm. (c) shows the detected line overlapped on the original kymograph with red and green lines showing anterogrades and retrogrades respectively.

The algorithm takes on an average 115 seconds for a kymograph. The length of false positives ridges and the length of ridges missed out by the algorithm are noted. From these, the percentage manual intervention is found to be around 10.83% which means that the algorithm is able to detect 89.17% of true ridges without manual efforts. The performance of the algorithm in extracting ridges when compared to 2 of the previous literatures is shown in 1 and 2. 10.83% of manual efforts is equivalent to spending 10 minutes whereas the manual analysis takes on an average 90 minutes for a kymograph. We have analysed the velocities of kymographs of *jsls821* strain (wild type) using the semi-automated method and compared the results with the manual method of analysis. Fig. 7 shows comparitive bar chart of mean velocities of manual and semi-automated method for anterogrades and retrogrades. A one-to-one comparison for each kymograph shows that the mean velocities are closer to those of manual method. Student's t-test assuming unequal variances was done for $\alpha = 0.05$. Out of 100 comparisons (50 anterogrades and 50 retrogrades), $p > \alpha$ for 88 cases. Manual delineation of the ridges yields piece-wise lines for each component. This leads to discrete set of velocities in the histogram plots as shown. With spline fitting, the histogram is smooth and most of the velocity components are clustered around the range specified by the biologists. A continuous

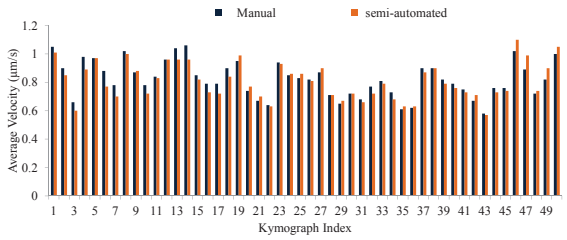

(a)

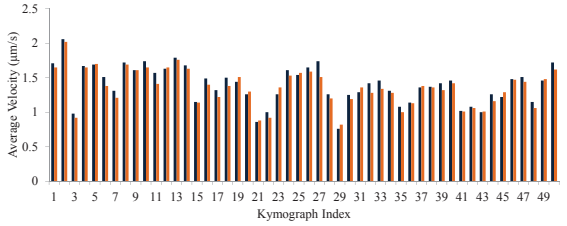

(b)

Fig. 7: (a) and (b) show the comparison of velocities from manual and computer assisted methods for anterogrades and retrogrades of 50 kymographs.

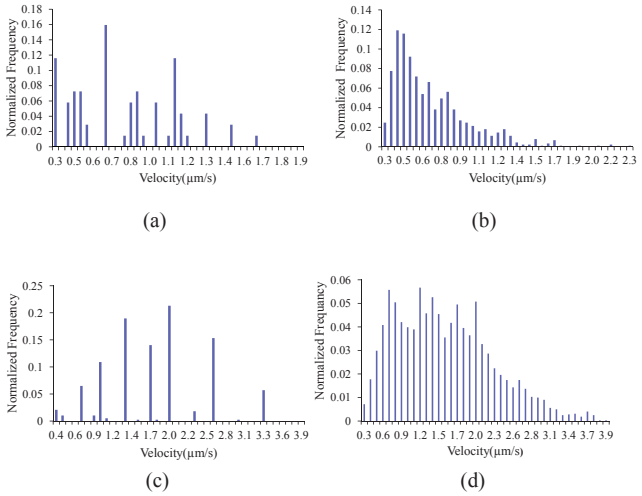

(a) (b) (c) (d)

Fig. 8: Comparison of normalized velocity distributions between the manual and computer assisted method for anterogrades and retrogrades of wild type kymographs. (a) and (b) show the manual results of anterogrades and retrogrades velocity respectively. (c) and (d) show the computer assisted results of anterogrades and retrogrades velocity respectively.

plot of histogram shows that the missed velocity bins in the manual analysis are captured by the automated spline fitting and velocity computation algorithm. The correctness of the automated method is confirmed by the Gaussian shape of the histogram clustered around the actual velocity range defined by the biologists for *C.elegans* (Fig. 8). The distribution of absolute error for anterogrades and retrogrades is shown in Fig. 9. The mean error for anterogrades is $0.03\mu m/s$ and retrogrades is $0.06\mu m/s$.

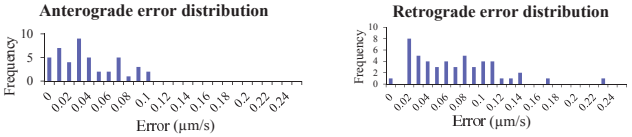

(a) (b)

Fig. 9: (a) and (b) show the absolute error distribution for anterogrades (mean error $0.03\mu m/s$) and retrogrades (mean error $0.06\mu m/s$) respectively. X axis shows error in $\mu m/s$. Y axis shows the number of kymographs. This shows that results of manual and semi-automated methods are closer to each other.

VI. Conclusion

We have developed a semi-automated algorithm for determining axonal transport velocities from kymographs. The algorithm based on LDA classifier, morphological image processing and spline fitting is a good alternative to manual analysis in terms of reduction in time taken by 89% with minimal differences in mean velocities, mean error being $0.03\mu m/s$ and $0.06\mu m/s$ for anterogrades and retrogrades respectively. In addition, our algorithm gives continuous instantaneous velocities which was not obtained with manual analysis. Our future work will focus on computing other metrics like pause time and pause frequency and developing a fully automated solution for axonal transport velocity estimation.

References

[1] Simon Andrews, Jonathan Gilley, and Michael P Coleman, "< i> difference tracker</i>: Imagej plugins for fully automated analysis of multiple axonal transport parameters," *Journal of neuroscience methods*, vol. 193, no. 2, pp. 281–287, 2010.

[2] Amit Mukherjee, Brian Jenkins, Cheng Fang, Richard J Radke, Gary Banker, and Badrinath Roysam, "Automated kymograph analysis for profiling axonal transport of secretory granules," *Medical image analysis*, vol. 15, no. 3, pp. 354–367, 2011.

[3] Oliver Welzel, Daniel Boening, Armin Stroebel, Udo Reulbach, Jurgen Klingauf, Johannes Kornhuber, and Teja Wolfgang Groemer, "Determination of axonal transport velocities via image cross-and autocorrelation," *European Biophysics Journal*, vol. 38, no. 7, pp. 883–889, 2009.

[4] Oliver Welzel, Jutta Knörr, Armin M Stroebel, Johannes Kornhuber, and Teja W Groemer, "A fast and robust method for automated analysis of axonal transport," *European Biophysics Journal*, vol. 40, no. 9, pp. 1061–1069, 2011.

[5] Minhua Qiu, Hao-Chih Lee, and Ge Yang, "Nanometer resolution tracking and modeling of bidirectional axonal cargo transport," in *Biomedical Imaging (ISBI), 2012 9th IEEE International Symposium on*. IEEE, 2012, pp. 992–995.

[6] Kai Zhang, Yasuko Osakada, Wenjun Xie, and Bianxiao Cui, "Automated image analysis for tracking cargo transport in axons," *Microscopy research and technique*, vol. 74, no. 7, pp. 605–613, 2011.

[7] Rangaraj M Rangayyan, Fábio J Ayres, Faraz Oloumi, Foad Oloumi, and Peyman Eshghzadeh-Zanjani, "Detection of blood vessels in the retina with multiscale gabor filters," *Journal of Electronic Imaging*, vol. 17, no. 2, pp. 023018–023018, 2008.

[8] Alejandro F Frangi, Wiro J Niessen, Koen L Vincken, and Max A Viergever, "Multiscale vessel enhancement filtering," in *Medical Image Computing and Computer-Assisted InterventationÂŰ-MICCAIÂŠ98*, pp. 130–137. Springer, 1998.

[9] Kyoko Chiba, Yuki Shimada, Masataka Kinjo, Toshiharu Suzuki, and Seiich Uchida, "Simple and direct assembly of kymographs from movies using kymomaker," *Traffic*, vol. 15, no. 1, pp. 1–11, 2014.